

Online Learning Feedback Control Considering Hysteresis for Musculoskeletal Structures

Kento Kawaharazuka¹, Kei Okada¹, and Masayuki Inaba¹

Abstract—While the musculoskeletal humanoid has various biomimetic benefits, its complex modeling is difficult, and many learning control methods have been developed. However, for the actual robot, the hysteresis of its joint angle tracking is still an obstacle, and realizing target posture quickly and accurately has been difficult. Therefore, we develop a feedback control method considering the hysteresis. To solve the problem in feedback controls caused by the closed-link structure of the musculoskeletal body, we update a neural network representing the relationship between the error of joint angles and the change in target muscle lengths online, and realize target joint angles accurately in a few trials. We compare the performance of several configurations with various network structures and loss definitions, and verify the effectiveness of this study on an actual musculoskeletal humanoid, Musashi.

I. INTRODUCTION

The musculoskeletal humanoid [1]–[3] has various biomimetic benefits such as the redundancy of its muscles [4], [5], variable stiffness mechanism with nonlinear elastic elements [6], ball joints without extreme points, and the under-actuated spine [3]. On the other hand, applying conventional control methods is unrealistic, because its complex body structure is difficult to modelize.

Therefore, several learning control methods have been developed so far. Mizuuchi, et al. have constructed a neural network which represents the relationship between joint angles and muscle lengths (joint-muscle mapping, JMM) from motion capture data, and realized target joint angles accurately [7]. Ookubo, et al. have expressed JMM by polynomials, and used it for the state estimation and control [8]. Kawaharazuka, et al. have developed a learning method of JMM by a neural network using vision [9] and its extended method considering the effect of muscle tensions [10]. However, because these methods use a one-to-one relationship between joint angles and muscle lengths, they cannot consider hysteresis of joint angle tracking, which makes realizing target joint angles accurately difficult.

To solve this problem, feedback control methods are considered. Mizuuchi, et al. have developed not only the feedforward but also the feedback control method of joint angles by the change in muscle lengths [7]. Motegi, et al. have developed a feedback control method of end-effector position by constructing a data table relating the end-effector position with muscle lengths [11]. However, when executing a feedback control at the fast frequency with the wrong

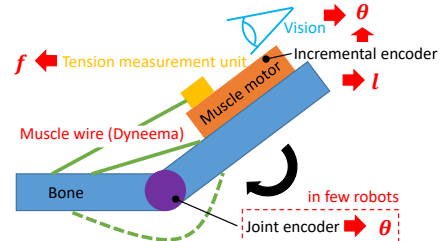


Fig. 1. Basic structure of the musculoskeletal humanoid.

muscle Jacobian, muscles can loosen or break due to high internal muscle tensions caused by its closed link structure. To avoid these problems, it is required to complete the feedback trial quickly or estimate its muscle Jacobian accurately. Although there are several methods estimating muscle Jacobian for musculoskeletal humanoids [10], [12], [13], there will always be some errors. Also, although there are methods to realize target posture using reinforcement learning [14], they are mostly performed in simulation only and are difficult to handle actual musculoskeletal humanoids with multiple degrees of freedom.

Therefore, we develop an online learning feedback control method (OLFC) considering hysteresis based on a muscle length-based control for the actual musculoskeletal humanoid. To realize target joint angles accurately in a few trials, we update a neural network representing the relationship between the error of joint angles and the change in target muscle lengths online and make use of it for the feedback control. This study can consider the time series motion transition of the actual musculoskeletal humanoid, as compared with the previous works of [7], [9]–[11]. Then, we compare the behaviors of OLFC using several experimental settings, network configurations, and loss definitions, in the actual robot experiment.

II. CHARACTERISTICS OF THE MUSCULOSKELETAL HUMANOID AND ITS BASIC FEEDBACK CONTROL

A. Basic Structure of the Musculoskeletal Humanoid

We show the basic body structure of the musculoskeletal humanoid in Fig. 1. Muscles are wound by pulleys using electrical motors and antagonistically arranged around joints. Muscle length l and tension f can be measured by encoders and loadcells, respectively. The abrasion resistant synthetic fiber Dyneema is used for the muscle wire, and it is slightly elastic. Depending on the robot, nonlinear elastic elements are attached to the endpoints of muscles to enable the variable stiffness control. Joint angles θ can be directly measured in few robots [15], [16]. However, even if the

¹ The authors are with the Department of Mechano-Informatics, Graduate School of Information Science and Technology, The University of Tokyo, 7-3-1 Hongo, Bunkyo-ku, Tokyo, 113-8656, Japan. [kawaharazuka, k-okada, inaba]@jsk.t.u-tokyo.ac.jp

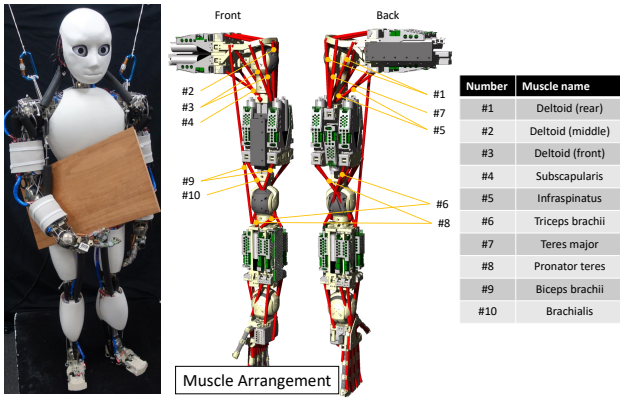


Fig. 2. A musculoskeletal humanoid Musashi [15] used in this study and the muscle arrangement of its left arm.

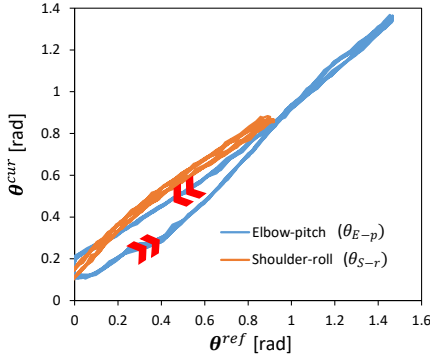


Fig. 3. Characteristics of hysteresis in the musculoskeletal structure.

robot has no joint angle sensors due to complex joints such as the scapula and shoulder ball joint, we can estimate the actual joint angles from changes in muscle lengths and vision information [9].

The musculoskeletal humanoid Musashi [15] used in this study is shown in the left figure of Fig. 2 and the muscle arrangement of its left arm is shown in the right figure of Fig. 2. Musashi has nonlinear elastic elements in muscles and joint angle sensors in joints to investigate and evaluate learning control systems. In this study, we mainly use the 3 DOF shoulder and 2 DOF elbow of the left arm of Musashi for experiments. We express these joint angles as $\theta = (\theta_{S-r}, \theta_{S-p}, \theta_{S-y}, \theta_{E-p}, \theta_{E-y})$ (S means the shoulder, E means the elbow, and rpy means the roll, pitch, and yaw angles, respectively). These 5 DOFs include 10 muscles (#1 – #10 in Fig. 2). Therefore, in experiments, \mathbf{f} and \mathbf{l} are 10 dimensional vectors, and θ is a 5 dimensional vector.

B. Characteristics of Hysteresis in the Musculoskeletal Structure

We conducted two experiments to investigate the characteristics of hysteresis in the musculoskeletal structure. First, we examined the tracking of the target joint angle $\theta^{ref} = \theta_{E-p}$ by changing it from 0 to -90 [deg] and from -90 to 0 [deg] over 10 sec and repeating this 10 times (we initialized the robot posture by $(\theta_{S-r}, \theta_{S-p}, \theta_{S-y}, \theta_{E-p}, \theta_{E-y}) = (0, 0, 0, 0, 0)$ [deg]). Second, we likewise examined the tracking of $\theta^{ref} = \theta_{S-r}$ by changing it from 0 to 60 [deg] and from 60 to 0 [deg] over 10 sec and repeating this 10 times. In these experiments,

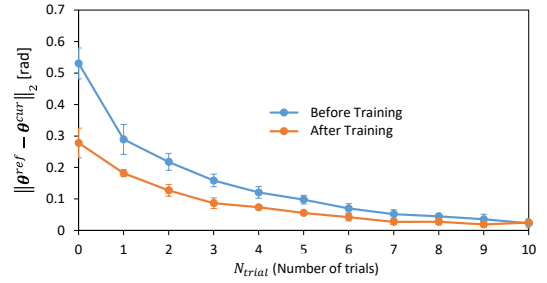


Fig. 4. Evaluation experiment of the basic feedback control using a network of [10]. This graph includes the results before and after the training of the network using the actual robot sensor information.

we converted the target joint angle θ^{ref} to the target muscle length l^{ref} using [10], and sent it to the actual robot.

We show the transition of θ^{ref} and the current joint angle θ^{cur} in Fig. 3. The graph of θ_{E-p} is turned over for better visual understandability. From these results, hysteresis exists in the joint angle movements. Its characteristics depend on joints such as $S - r$ and $E - p$, and the hysteresis has reproducibility because there is almost no difference among the 10 repeated movements.

C. Basic Feedback Control

As the simplest way to solve the hysteresis problem, we show the basic feedback control method (BFC) [7]. We execute BFC using not the original network $h_{orig}(\theta)$ in [7] but the latest network $h(\theta, \mathbf{f})$ in [9], which can be trained using the actual robot sensor information. In BFC, the target change in muscle length Δl , when given the current joint angle θ^{cur} and the target joint angle θ^{ref} , is calculated as below,

$$\Delta l(\theta^{ref}, \theta^{cur}) = h(\theta^{ref}, \mathbf{f}^{cur}) - h(\theta^{cur}, \mathbf{f}^{cur}) \quad (1)$$

where \mathbf{f}^{cur} is the current muscle tension. In Eq. 1, we assume that θ^{cur} is close to θ^{ref} and so \mathbf{f}^{cur} is not largely changed by sending Δl . θ^{ref} is realized to some extent by $l^{ref} = h(\theta^{ref}, \mathbf{f}_{const})$ first (\mathbf{f}_{const} is a certain constant value; 30 N in this study), and θ^{ref} is accurately realized by repeating Eq. 1 as $l^{ref} \leftarrow l^{ref} + \Delta l$.

D. The Evaluation of Basic Feedback Control

We evaluated BFC in an actual robot experiment by repeating the N_{trial}^{max} times execution of Eq. 1 N_{rand}^{max} times. We conducted an experiment to realize the target joint angle θ^{ref} of $(\theta_{S-r}, \theta_{S-p}, \theta_{S-y}, \theta_{E-p}, \theta_{E-y}) = (30, -30, 30, -60, 30)$ [deg] from 5 randomly chosen joint angles θ_{rand} . First, the target joint angle is realized by $l^{ref} = h(\theta^{ref}, \mathbf{f}_{const})$ to some extent. Then, the trial is set as $N_{trial} = 0$, and $\|\theta^{ref} - \theta^{cur}\|_2$ ($\|\cdot\|_2$ expresses L2 norm) is measured every time Eq. 1 is performed. Eq. 1 is quasi-statically executed over 3 sec. By repeating Eq. 1 N_{trial}^{max} times ($0 \leq N_{trial} < N_{trial}^{max}$) from θ^{cur} to θ^{ref} while changing the initial posture θ_{rand} N_{rand}^{max} times ($0 \leq N_{rand} < N_{rand}^{max}$), we check the average and variance of $\|\theta^{ref} - \theta^{cur}\|_2$ of N_{rand}^{max} times at the N_{trial} -th trial. We set $N_{trial}^{max} = 10$ and $N_{rand}^{max} = 5$ in this experiment.

The graph in Fig. 4 shows the result of conducting Eq. 1 using h , before and after its training using the actual

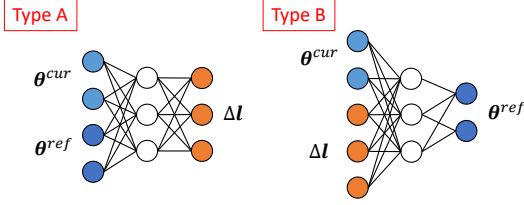


Fig. 5. Network structures for online learning feedback control.

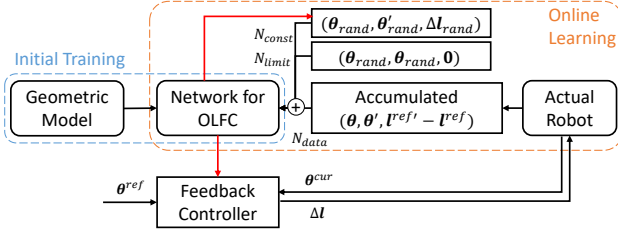


Fig. 6. The overall system of this study.

robot sensor information in [10]. After the training of \mathbf{h} , $\|\theta^{ref} - \theta^{cur}\|_2$ at $N_{trial} = 0$ drops by half compared to the result before the training of \mathbf{h} . Although the final results of $\|\theta^{ref} - \theta^{cur}\|_2$ do not largely vary, the convergence is faster after the training of \mathbf{h} than before it. However, both require many trials to converge, and the current learning method training one-to-one relationship between joint angles and muscle lengths is not enough.

The method of BFC does not consider hysteresis. Thus, $\Delta l(\theta_1, \theta_2) = \Delta l(\theta_2, \theta_1)$, when setting the random joint angles of θ_1 and θ_2 . However, because hysteresis exists as shown in Section II-B, the target joint angle cannot be easily realized, the number of trials of Eq. 1 increases, and muscles can loosen or high muscle tension can emerge as stated in Section I. To realize the target joint angle in a few trials of feedback control, we propose online learning feedback control next.

III. ONLINE LEARNING FEEDBACK CONTROL

In this section, we will propose a method to acquire the target change in muscle length Δl to realize θ^{ref} from θ^{cur} by online learning. We will explain two different network structures for the purpose, their initial training and online learning, and feedback controls using the trained networks.

A. Network Structures

We can consider two neural network structures for online learning feedback control (OLFC) shown in Fig. 5. These structures are chosen by considering all combinations of θ^{cur} , θ^{ref} , and Δl as network input and output, and only the chosen two networks are valid. First, the simplest network structure to realize our objective (\mathbf{h}_A , Type A) is represented as below.

$$\Delta l = \mathbf{h}_A(\theta^{cur}, \theta^{ref}) \quad (2)$$

By using Type A, Δl can be directly calculated when given θ^{cur} and θ^{ref} . Second, when examining the relationship among θ^{cur} , θ^{ref} , and Δl , we can consider a network structure representing the transition of joint angles with the change in muscle length (\mathbf{h}_B , Type B), as below.

$$\theta^{ref} = \mathbf{h}_B(\theta^{cur}, \Delta l) \quad (3)$$

By using a backpropagation [17] and gradient descent method for the inputs, Δl can also be calculated from θ^{cur} and θ^{ref} . We show the overall system of this study in Fig. 6.

B. Initial Training of the Networks

We collect the data of $(\theta^{cur}, \theta^{ref}, \Delta l)$ using a geometric model and train the networks. The geometric model has information about joint position, link length, and link weight. Also, each muscle route is expressed by linearly connecting its start point, relay points, and end point. By setting a certain joint angle, muscle length can be calculated from the distance of the start, relay, and end points. This geometric model is designed by humans, and cannot consider the muscle wrapping around the skeleton, the elongation of the muscle wire, hysteresis, etc.

First, we calculate the muscle length l at a random joint angle θ from the geometric model. Second, we calculate the muscle length l' at the joint angle of $\theta' = \theta + \Delta\theta$. In this procedure, $\Delta\theta$ is a random value following a normal distribution with an average of 0 and a standard deviation of $S_{\Delta\theta}$ ($S_{\Delta\theta} = 0.5$ [rad] in this study). Then, we can construct a dataset of $(\theta^{cur} = \theta, \theta^{ref} = \theta', \Delta l = l' - l)$ by repeating the above procedure, and train these networks using it. In this study, each network has 5 fully-connected layers including the input and output layers, and the numbers of units in the hidden layers are (40, 20, 20). Also, the loss function is a mean squared error, the activation function is Sigmoid, and the optimization method is Adam [18].

C. Online Learning of the Network

First, a joint angle movement from the previous joint angle θ to the current joint angle θ' is detected using the change in target muscle length from l^{ref} to $l^{ref'}$. Then, the data of $(\theta^{cur} = \theta, \theta^{ref} = \theta', \Delta l = l^{ref'} - l^{ref})$ can be obtained. Because of the assumption that θ is close to θ' as stated in Section II-C, the data is used only when $\|\theta - \theta'\|_2 < C_{length}$ (C_{length} is a threshold constant). We repeat this step, accumulate the data, and start the online learning when the number of the accumulated data exceeds a threshold value N_{thre} . We choose N_{data} (N_{data} is a constant, $N_{data} \leq N_{thre}$) number of data from these accumulated data and add them into a batch for online learning. In order to add the limitation of “ $\Delta l = 0$ when $\theta^{cur} = \theta^{ref}$ ”, we add N_{limit} number of data $(\theta_{rand}, \theta_{rand}, 0)$ into the batch by randomly choosing θ_{rand} (N_{limit} is a constant). Also, the network should not be changed except for around the obtained data. Thus, regarding Type A, we add N_{const} number of data into the batch (N_{const} is a constant), by calculating Δl_{rand} from the randomly chosen θ_{rand} and θ'_{rand} using the current network. Regarding Type B, we likewise calculate θ'_{rand} from the randomly chosen θ_{rand} and Δl_{rand} . Finally, we set the number of epochs as N_{epoch} and the batch size as $N_{data} + N_{limit} + N_{const}$, which is the sum of the data stated above, and train the network. In this study, we set $C_{length} = 100$ [mm], $N_{thre} = 10$, $N_{data} = 10$, $N_{limit} = 5$, $N_{const} = 5$, and $N_{epoch} = 3$.

D. Feedback Control Using the Learned Network

The network of Type A is the simplest, and we can obtain Δl through the network by merely measuring θ^{cur} and deciding θ^{ref} .

On the other hand, several procedures to obtain Δl are required for the network of Type B. First, we calculate the original target change in muscle length Δl_{geo} using the geometric model as shown below,

$$\Delta l_{geo} = h_{geo}(\theta^{ref}) - h_{geo}(\theta^{cur}) \quad (4)$$

where h_{geo} is the mapping from joint angle to muscle length in the geometric model. Δl_{geo} is almost the same value as the output of Eq. 1 before the training of h in [10]. Second, we obtain the predicted joint angle θ^{pred} by feeding θ^{cur} and Δl_{geo} into the network of Type B. Then, we define the loss function L as shown below, and update Δl_{geo} through backpropagation [17] and descent gradient method,

$$L_0 = \|\theta^{pred} - \theta^{ref}\|_2 \quad (5)$$

$$\Delta l_{geo} \leftarrow \Delta l_{geo} - \gamma \partial L / \partial \Delta l_{geo} \quad (6)$$

where γ is a learning rate. Although we can set γ as a constant value, we change γ variously for better convergence. We decide the maximum value of γ as γ_{max} , equally divide $[0, \gamma_{max}]$ into N_{batch} parts, update Δl_{geo} by each learning rate, and choose the one with the minimum loss L when feeding it into the network again. By repeating these procedures and updating Δl_{geo} , N_{update} times (N_{update} is a constant), we can finally obtain the refined Δl_{geo} as the target Δl .

This method has some extensions. For example, by defining L as shown below and executing the same procedure as stated above, we can calculate Δl to realize θ^{ref} with the minimum change in muscle length,

$$L_1 = \|\theta^{pred} - \theta^{ref}\|_2 + \alpha \|\Delta l\|_2 \quad (7)$$

where α is a weight coefficient. Similarly, by defining L as shown below, we can inhibit only the contracting muscles and avoid high internal muscle tension.

$$\Delta l_{processed} = \begin{cases} \Delta l, & \text{if } \Delta l < 0 \\ 0, & \text{else} \end{cases} \quad (8)$$

$$L_2 = \|\theta^{pred} - \theta^{ref}\|_2 + \alpha \|\Delta l_{processed}\|_2 \quad (9)$$

In this study, we set $\gamma_{max} = 10$ [mm], $N_{batch} = 10$, $N_{update} = 10$, and $\alpha = 0.0003$, and we use Eq. 5 as the loss function unless otherwise noted.

IV. EXPERIMENTS

First, we will conduct OLFC using the network of Type A and B, and compare the convergence of joint angles between θ^{cur} and θ^{ref} among these networks. Second, we will compare the difference in the behavior of OLFC among the different loss definitions and among different situations such as changing the posture or grasping a heavy object. Also, we will conduct a quantitative evaluation of OLFC. Finally, we will conduct a practical task of Japanese stamp pushing using the proposed method and visual information.

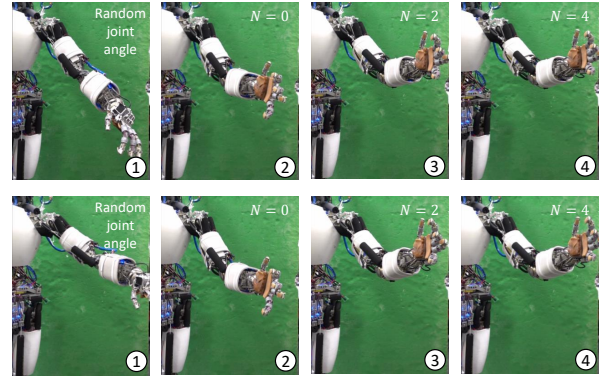


Fig. 7. The experiment of online learning feedback control.

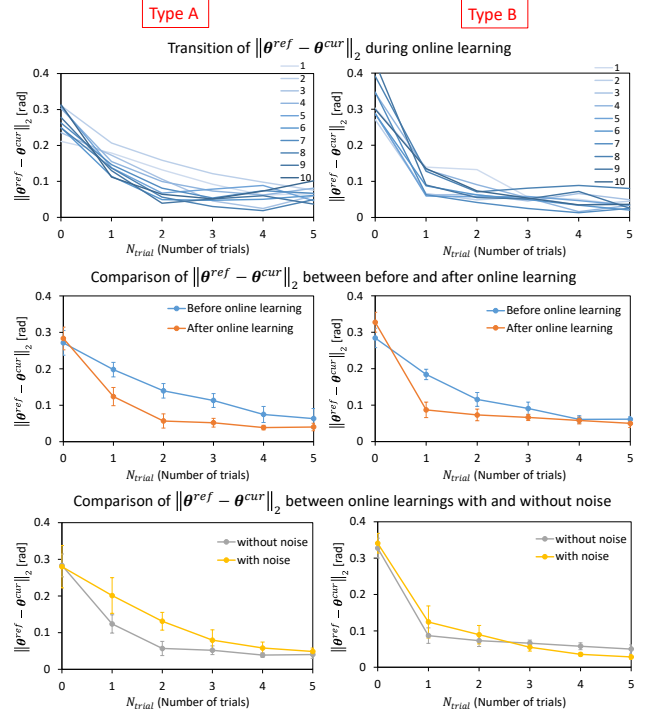


Fig. 8. Comparison of online learning feedback controls between using the networks of Type A and Type B.

In this section, we will mainly conduct experiments to realize the target joint angle θ^{ref} from the randomly chosen joint angle θ_{rand} , as in Section II-D. First, we realize the target joint angle by $l^{ref} = h(\theta^{ref}, f_{const})$ to some extent (h is already trained). Then, setting the trial as $N_{trial} = 0$, we measure $\|\theta^{ref} - \theta^{cur}\|_2$, conducting OLFC stated in Section III-D every time. By repeating OLFC N_{trial}^{max} times ($0 \leq N_{trial} < N_{trial}^{max}$) from θ^{cur} to θ^{ref} while changing the initial posture θ_{rand} N_{rand}^{max} times ($0 \leq N_{rand} < N_{rand}^{max}$), we check the average and variance of $\|\theta^{ref} - \theta^{cur}\|_2$ of N_{rand}^{max} times at the N_{trial} -th trial. We express this graph as $\text{Graph}_{ave}(\theta^{ref}, N_{trial}^{max}, N_{rand}^{max})$. Also, $\text{Graph}_{raw}(\theta^{ref}, N_{trial}^{max}, N_{rand}^{max})$ expresses N_{rand}^{max} times the transition of $\|\theta^{ref} - \theta^{cur}\|_2$ without averaging them. Here, all constants are defined as with the preliminary experiment in Section II-D.

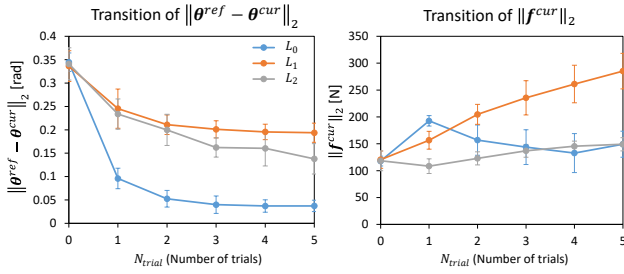


Fig. 9. Comparison of online learning feedback controls among various loss definitions.

A. Learning Feedback Control with Different Network Structures

By setting θ^{ref} as a certain joint angle $\theta_0 = (\theta_{S-r}, \theta_{S-p}, \theta_{S-y}, \theta_{E-p}, \theta_{E-y}) = (30, -30, 30, -60, 30)$ [deg], we compare OLFC using the networks of Type A and B in the same experiment.

We show the experiment in Fig. 7 and the experimental results in Fig. 8. In the upper graphs of Fig. 8, we show $\text{Graph}_{raw}(\theta^{ref} = \theta_0, N_{trial}^{max} = 5, N_{rand}^{max} = 10)$ during online learning stated in Section III-C. While $\|\theta^{ref} - \theta^{cur}\|_2$ regarding Type A gradually decreases as N_{rand} increases, the online learning regarding Type B converges after a few N_{rand} .

The middle graphs of Fig. 8 show $\text{Graph}_{ave}(\theta^{ref} = \theta_0, N_{trial}^{max} = 5, N_{rand}^{max} = 5)$ before and after the online learning. In subsequent experiments, the online learning procedure is not working when conducting comparison experiments. We can see that the convergence of joint angles is improved very much regarding both Type A and B. $\|\theta^{ref} - \theta^{cur}\|_2$ regarding Type B converges more quickly than Type A.

Finally, we discuss the difference between Type A and B, and conduct a comparative experiment. The transition of joint angles in the network of Type B holds true at all times but it does not necessarily hold regarding Type A. In the case of the redundant flexible musculoskeletal structure, we can consider various Δl to realize θ^{ref} from θ^{cur} , and the result of the online learning should depend on the training data. So we conduct the same experiments as stated above with added noise to the data for online learning, as shown below,

$$\Delta l \leftarrow \Delta l + \text{Random}(a, b) \quad (10)$$

where $\text{Random}(a, b)$ is the random value in $[a, b]$ ($a = 0, b = 5$ [mm] in this study). We show $\text{Graph}_{ave}(\theta^{ref} = \theta_0, N_{trial}^{max} = 5, N_{rand}^{max} = 5)$ with or without the additional noise during the online learning in the lower graphs of Fig. 8. While the result of the online learning does not vary with or without the additional noise regarding Type B, the convergence largely deteriorates regarding Type A and its variance is comparatively large.

We use the network of Type B in remaining experiments.

B. Learning Feedback Control with Various Loss Definition

As stated in Section III-D, regarding Type B, we can change the behavior of OLFC by changing the definition of L . We show the difference of $\text{Graph}_{ave}(\theta^{ref} = \theta_0, N_{trial}^{max} = 5, N_{rand}^{max} = 5)$ among the loss definitions of L_0 (Eq. 5), L_1 (Eq.

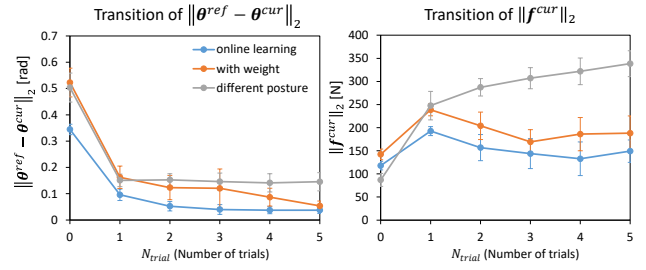


Fig. 10. Comparison of online learning feedback controls among various situations

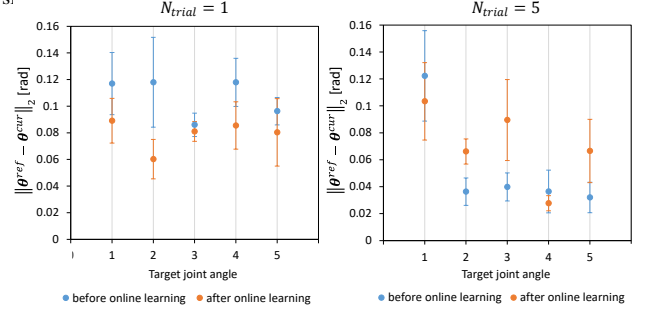


Fig. 11. Quantitative evaluation of online learning feedback control.

7), and L_2 (Eq. 9) in the left graph of Fig. 9. In the right graph of Fig. 9, we show $\|\mathbf{f}^{cur}\|_2$ instead of $\|\theta^{ref} - \theta^{cur}\|_2$ regarding Graph_{ave} (\mathbf{f}^{cur} is the current muscle tension). We can see that the results using L_1 and L_2 deteriorate compared to L_0 , due to the additional limitation of Δl . Also, the result of L_2 is better than that of L_1 . Regarding $\|\mathbf{f}^{cur}\|_2$, while the muscle tension gradually increases when using L_1 , the muscle tension does not vary much when using L_2 . When using L_0 , the muscle tension increases in the beginning, but gradually decreases afterwards. However, the variance of the muscle tension is large, and so high muscle tension sometimes emerges.

C. Learning Feedback Control in Various Situations

We verify whether the online learning result is valid in situations different from those when conducting the online learning. As in Section IV-A, we conducted the online learning by setting $N_{trial}^{max} = 5, N_{rand}^{max} = 10$. We verified the difference of $\text{Graph}_{ave}(\theta^{ref} = \theta_0, N_{trial}^{max} = 5, N_{rand}^{max} = 5)$ among the state with online learning, the state grasping a heavy object (3.6 kg), and the state with a forward-bent posture (45 deg). During these experiments, the online learning was not executed. As with Section IV-B, we also checked $\|\mathbf{f}^{cur}\|_2$. The result is shown in Fig. 10. By grasping the heavy object or changing the posture, $\|\theta^{ref} - \theta^{cur}\|_2$ deteriorates at $N_{trial} = 0$, because the space of muscle tension which is not trained by [10] is used. However, even with changes in situation, the convergence is faster than before the online learning. In the left graph of Fig. 10, we can see that the muscle tension increases as a whole when grasping the heavy object. Also, when changing the posture, the joint torque is insufficient, high muscle tension emerges, and the convergence stops at a certain value.

D. Quantitative Evaluation of Learning Feedback Control

So far, we have verified OLFC regarding only one certain joint angle by setting $\theta^{ref} = \theta_0$. In this experiment, we will

evaluate OLFC quantitatively for movements that realize the randomly chosen various joint angles. First, we randomly generated 5 target joint angles θ^{ref} for evaluation. We conducted the feedback control experiment to realize each θ^{ref} by setting $N_{trial}^{max} = 5$ and $N_{rand}^{max} = 5$. Second, we conducted the feedback control experiment to realize the random joint angle θ'_{rand} from the random joint angle θ_{rand} by setting $N_{trial}^{max} = 5$ and $N_{rand}^{max} = 20$, while running the online learning. Finally, we conducted the same experiment as before online learning to realize each θ^{ref} by setting $N_{trial}^{max} = 5$ and $N_{rand}^{max} = 5$.

We show the average and variance of $\|\theta^{ref} - \theta^{cur}\|_2$ of N_{rand}^{max} times at $N_{trial} = 1$ and $N_{trial} = 5$ regarding each θ^{ref} before and after the online learning in Fig. 11. Regarding $N_{trial} = 1$, the precision after the online learning is better than before the online learning at any θ^{ref} , even if θ^{ref} is not included in θ'_{rand} . On the other hand, regarding $N_{trial} = 5$, the precisions before and after the online learning do not largely vary. There are many cases where the variance before the online learning is better than that after the online learning.

E. Japanese Stamp Pushing Experiment

We will conduct a practical task of pushing a Japanese stamp, integrating the proposed method and visual information. We put an AR marker on the desk, and the robot pushes a Japanese stamp at the position x_{place} which is 50 mm from the marker toward the robot. Also, as stated in Section II-A, we estimated the actual joint angle from the vision sensor using the method of [9]. This is a method to estimate the actual joint angle θ^{est} by attaching an AR marker to the hand, setting the estimated joint angle from muscle length as the initial joint angle, and solving inverse kinematics to the marker. Since the link length and joint position of the geometric model are not necessarily correct, we can conduct the position alignment more precisely by using θ^{est} . The current position of the Japanese stamp is expressed as x^{cur} calculated from the obtained θ^{est} . Similarly, by setting θ^{est} as the initial joint angle and solving inverse kinematics to x^{ref} (we will explain x^{ref} below), we obtain the target joint angle θ^{ref} . In this experiment, we do not conduct the movement at $N_{trial} = 0$ as in previous experiments, but conduct only the feedback control to realize θ^{ref} from $\theta^{cur} = \theta^{est}$, and evaluate $\|x^{ref} - x^{cur}\|_2$ at each step. In the beginning, the robot with a Japanese stamp moves its arm to 50 mm above x_{place} by OLFC, and after that, sets the stamp down to x_{place} . Finally, by changing the rotation of the arm at x_{place} several times, the robot firmly pushes the Japanese stamp.

We show the experiment and transition of $\|x^{ref} - x^{cur}\|_2$ in Fig. 12. In this experiment, x^{ref} is the position 50 mm above x_{place} . The case after online learning shows a better convergence than before online learning. Although the stamp was firmly pushed, the stamp contacted the paper before convergence when moving to x_{place} from x^{ref} , and it was difficult to push the stamp at the exact place.

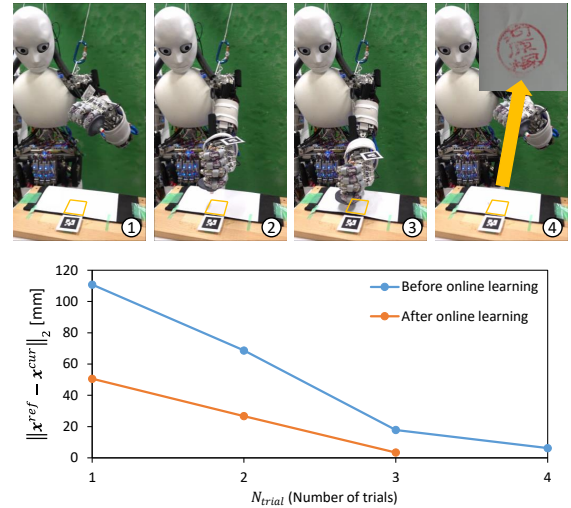


Fig. 12. Experiment of pushing a Japanese stamp by visual feedback.

V. DISCUSSION

A. Experimental Results

In Section IV-A, we found that the convergence of online learning is faster for Type B, which represents the transition of the joint angle, than for Type A, which calculates the target change in muscle length from two joint angles. After online learning, the error of the feedback control drops gently for Type A, while it drops sharply for Type B. Also, the performance of Type A deteriorates markedly when the noise is added to the feedback control, while the performance of Type B does not change at all. This means that the convergence of the model by online learning and the convergence of the joint angle error by the feedback control using the learned model are better for Type B than for Type A. It is important to note that Type A does not necessarily hold true while Type B holds true at all times, which may contribute significantly to the performance of the network.

In Section IV-B, we found that the loss of minimizing Δl prevents the antagonist muscles from loosening and increases the internal force in L_1 . In contrast, L_2 avoids the increase in muscle tension compared to L_0 , although its accuracy is lower. Therefore, L_0 is useful when accuracy is emphasized and L_2 is also useful when the increase in muscle tension should be avoided.

In Section IV-C, we found that the convergence of the joint angle errors after learning is faster than that before learning and that this method is useful, even in different situations.

In Section IV-D, we found that the accuracy after online learning is better for $N_{trial} = 1$ than before online learning, while there is no significant difference in the accuracy before and after the learning for $N_{trial} = 5$. We can consider that this is because learning globally is easy, but the online learning is difficult when $\|\theta^{cur} - \theta^{ref}\|_2$ is small. Therefore, it is important to use this method for a very small number of feedback trials.

In Section IV-E, we found that the position error after learning is better converged than before learning. Visual feedback can be constructed by combining visual information

and the proposed feedback control, and that this study can be applied to musculoskeletal humanoids without joint angle sensors, using θ^{est} .

B. Limitations and Future Works

Our method has the following limitations: (i) it assumes quasi-static behavior, and (ii) it does not completely reduce the joint angle error to zero.

As for (i), if the robot moves at high speed, the assumption of the network does not hold and the proposed method may not be applied well. On the other hand, although dynamic effects can be considered by the recurrent network structure at high frequency, there are some problems such as a large amount of data and difficulty in learning a large space of time series data. Therefore, it is necessary to develop more efficient sampling and learning methods.

As for (ii), this feedback control does not realize the target joint angle as accurately as the feedback control in the axis-driven type. This characteristic is important, and we realize that a new paradigm of control for musculoskeletal humanoids is required, as well as the accurate realization of the joint angle as in this study. We would like to establish a control method to accomplish the task by making full use of various environments and tools, no matter how much the joint angle error is.

VI. CONCLUSION

In this study, we proposed an online learning feedback control system considering hysteresis of musculoskeletal structures, and compared its network structures and loss definitions. By constructing a network that represents the transition of the current joint angle by the change in muscle length, we can calculate the optimized change in muscle length to realize the target joint angle through backpropagation and gradient descent. The convergence of the feedback control using this network is better than that of using the network with the current and target joint angles as the input and the change in muscle length as the output. We can inhibit high internal muscle tension by changing the definition of the loss function. Also, this method can work in situations different from those of the online learning, such as with external force or with different posture, and is shown to have a generalization ability from the quantitative experiment. This method can be applied to the musculoskeletal humanoid without joint angle sensors, and we can conduct visual feedback by using vision sensor.

REFERENCES

- [1] S. Wittmeier, C. Alessandro, N. Bascarevic, K. Dalamagkidis, D. Devereux, A. Diamond, M. Jäntsch, K. Jovanovic, R. Knight, H. G. Marques, P. Milosavljevic, B. Mitra, B. Svetozarevic, V. Potkonjak, R. Pfeifer, A. Knoll, and O. Holland, "Toward Anthropomorphic Robotics: Development, Simulation, and Control of a Musculoskeletal Torso," *Artificial Life*, vol. 19, no. 1, pp. 171–193, 2013.
- [2] M. Jäntsch, S. Wittmeier, K. Dalamagkidis, A. Panos, F. Volkart, and A. Knoll, "Anthrob - A Printed Anthropomorphic Robot," in *Proceedings of the 2013 IEEE-RAS International Conference on Humanoid Robots*, 2013, pp. 342–347.
- [3] Y. Asano, T. Kozuki, S. Ookubo, M. Kawamura, S. Nakashima, T. Katayama, Y. Iori, H. Toshinori, K. Kawaharazuka, S. Makino, Y. Kakiuchi, K. Okada, and M. Inaba, "Human Mimetic Musculoskeletal Humanoid Kengoro toward Real World Physically Interactive Actions," in *Proceedings of the 2016 IEEE-RAS International Conference on Humanoid Robots*, 2016, pp. 876–883.
- [4] K. Kawaharazuka, A. Miki, Y. Toshimitsu, K. Okada, and M. Inaba, "Adaptive Body Schema Learning System Considering Additional Muscles for Musculoskeletal Humanoids," *IEEE Robotics and Automation Letters*, vol. 7, no. 2, pp. 3459–3466, 2022.
- [5] K. Kawaharazuka, M. Nishiura, Y. Toshimitsu, Y. Omura, Y. Koga, Y. Asano, K. Okada, K. Kawasaki, and M. Inaba, "Robust Continuous Motion Strategy Against Muscle Rupture using Online Learning of Redundant Intersensory Networks for Musculoskeletal Humanoids," *Robotics and Autonomous Systems*, vol. 152, pp. 1–14, 2022.
- [6] K. Kawaharazuka, K. Tsuzuki, S. Makino, M. Onitsuka, Y. Asano, K. Okada, K. Kawasaki, and M. Inaba, "Long-time Self-body Image Acquisition and its Application to the Control of Musculoskeletal Structures," *IEEE Robotics and Automation Letters*, vol. 4, no. 3, pp. 2965–2972, 2019.
- [7] I. Mizuuchi, Y. Nakanishi, T. Yoshikai, M. Inaba, H. Inoue, and O. Khatib, "Body Information Acquisition System of Redundant Musculo-Skeletal Humanoid," in *Experimental Robotics IX*, 2006, pp. 249–258.
- [8] S. Ookubo, Y. Asano, T. Kozuki, T. Shirai, K. Okada, and M. Inaba, "Learning Nonlinear Muscle-Joint State Mapping Toward Geometric Model-Free Tendon Driven Musculoskeletal Robots," in *Proceedings of the 2015 IEEE-RAS International Conference on Humanoid Robots*, 2015, pp. 765–770.
- [9] K. Kawaharazuka, S. Makino, M. Kawamura, Y. Asano, K. Okada, and M. Inaba, "Online Learning of Joint-Muscle Mapping using Vision in Tendon-driven Musculoskeletal Humanoids," *IEEE Robotics and Automation Letters*, vol. 3, no. 2, pp. 772–779, 2018.
- [10] K. Kawaharazuka, S. Makino, M. Kawamura, A. Fujii, Y. Asano, K. Okada, and M. Inaba, "Online Self-body Image Acquisition Considering Changes in Muscle Routes Caused by Softness of Body Tissue for Tendon-driven Musculoskeletal Humanoids," in *Proceedings of the 2018 IEEE/RSJ International Conference on Intelligent Robots and Systems*, 2018, pp. 1711–1717.
- [11] Y. Motegi, T. Shirai, T. Izawa, T. Kurotobi, J. Urata, Y. Nakanishi, K. Okada, and M. Inaba, "Motion control based on modification of the Jacobian map between the muscle space and work space with musculoskeletal humanoid," in *Proceedings of the 2012 IEEE-RAS International Conference on Humanoid Robots*, 2012, pp. 835–840.
- [12] V. D. Sapio, K. Holzbaur, and O. Khatib, "The control of kinematically constrained shoulder complexes: physiological and humanoid examples," in *Proceedings of the 2006 IEEE International Conference on Robotics and Automation*, 2006, pp. 2952–2959.
- [13] M. Jäntsch, S. Wittmeier, K. Dalamagkidis, G. Herrmann, and A. Knoll, "Adaptive neural network Dynamic Surface Control: An evaluation on the musculoskeletal robot Anthrob," in *Proceedings of the 2015 IEEE International Conference on Robotics and Automation*, 2015, pp. 4347–4352.
- [14] A. Diamond and O. E. Holland, "Reaching control of a full-torso, modelled musculoskeletal robot using muscle synergies emergent under reinforcement learning," *Bioinspiration & Biomimetics*, vol. 9, no. 1, pp. 1–16, 2014.
- [15] K. Kawaharazuka, S. Makino, K. Tsuzuki, M. Onitsuka, Y. Nagamatsu, K. Shinjo, T. Makabe, Y. Asano, K. Okada, K. Kawasaki, and M. Inaba, "Component Modularized Design of Musculoskeletal Humanoid Platform Musashi to Investigate Learning Control Systems," in *Proceedings of the 2019 IEEE/RSJ International Conference on Intelligent Robots and Systems*, 2019, pp. 7294–7301.
- [16] J. Urata, Y. Nakanishi, A. Miyadera, I. Mizuuchi, T. Yoshikai, and M. Inaba, "A Three-Dimensional Angle Sensor for a Spherical Joint Using a Micro Camera," in *Proceedings of the 2006 IEEE International Conference on Robotics and Automation*, 2006, pp. 4428–4430.
- [17] D. E. Rumelhart, G. E. Hinton, and R. J. Williams, "Learning representations by back-propagating errors," *nature*, vol. 323, no. 6088, pp. 533–536, 1986.
- [18] D. P. Kingma and J. Ba, "Adam: A Method for Stochastic Optimization," in *Proceedings of the 3rd International Conference on Learning Representations*, 2015, pp. 1–15.